



Effects of the airfoil section, the chord and pitch distributions on the aerodynamic performance of the propeller

Kamal A. R. Ismail¹ · Célia V. A. G. Rosolen¹

Received: 2 July 2018 / Accepted: 1 February 2019
© The Brazilian Society of Mechanical Sciences and Engineering 2019

Abstract

The main objectives of this study are to investigate parametrically the possible use of alternative airfoils (Joukowski and Göttingen) for propellers and to assess the effects of varying the chord and pitch angle distributions as well as the use of multiple airfoils along the blade on the performance parameters of the propeller. In this study, a validated home-built FORTRAN code based on the BEM method with incorporated tip and compressibility losses is used. The detailed investigation of the blade geometry is done to help in selecting a configuration that is efficient and easy to manufacture. The linear pitch distribution is found to reduce the coefficients of thrust and power as well as higher blade loading at the intermediate region and lower loading at the tip region in comparison with the Göttingen 796-based propeller. The results show that the power coefficient and efficiency of the generalized Joukowski-based propeller are greater than the respective coefficients of Göttingen 796-based propeller for advanced ratio $J=0.85$ and higher. The predicted results indicate that the use of the elliptical chord distribution provokes reduction in the blade loading at the tip region and increases at the intermediate region of the blade. It is found also that it reduces the coefficient of thrust, torque and power in comparison with the blade having the reference chord distribution.

Keywords Small propeller · Momentum theory · Blade element theory · Panel method · Blade aerodynamics · Airfoil section

List of symbols

a	Inflow factor
a_0	Lift curve slope at zero Mach number (i.e., in incompressible flow) (radians ⁻¹)
a_M	Lift curve slope at zero Mach number (radians ⁻¹)
b	Swirl factor
B	Number of blades of the propeller
c	Local blade chord (m)
C_d	Two-dimensional drag coefficient of the local blade chord

C_1	Two-dimensional lift coefficient of the local blade chord
D	Diameter of the propeller (m)
f_{tip}	Tip loss correction used to calculate Prandtl loss factor F
f_{hub}	Hub loss correction used to calculate Prandtl loss factor F
F	Prandtl loss factor for combined tip and hub losses which arise due to the finite number of the propeller blades
J	Advance ratio of the propeller $J = V/(nD)$
k_P	Power coefficient of the propeller $k_P = P/(\rho n^3 D^5)$
k_Q	Torque coefficient of the propeller $k_Q = Q/(\rho n^2 D^5)$
k_T	Thrust coefficient of the propeller $k_T = T/(\rho n^2 D^4)$
M	Local Mach number of the relative flow
n	Rotational speed of the propeller (rps)
N	Rotational speed of the propeller (rpm)
p	Geometric pitch of the blade section (m)
P	Power supplied at the propeller axis (Nm/s)
Q	Torque applied on the propeller (Nm)
r	Radius of the transversal section of the blade of the propeller (m)

Technical Editor: André Cavalieri.

✉ Kamal A. R. Ismail
kamal@fem.unicamp.br
Célia V. A. G. Rosolen
c.rosolen@uol.com.br

¹ Department of Energy, School of Mechanical Engineering, University of Campinas, Rua Mendeleiev, 200, Cidade Universitária “Zeferino Vaz”, Campinas, SP 13083-860, Brazil

R	Radius of the blade tip of the propeller (m)
Re_{75}	Reynolds number of the propeller based on the local chord and resultant velocity at a radial distance of 0.75 of the tip radius
T	Thrust force of the propeller (N)
V	Advance velocity of the propeller (m/s)
V_0	Axial component of the flow velocity relative to the blade (m/s)
V_R	Resultant flow velocity relative to the blade (m/s)
V_S	Axial component of the flow velocity relative to the propeller at exit of the slipstream (m/s)
V_w	Rotational component of the flow velocity relative to blade (m/s)
α	Angle of attack is the angle between the resultant velocity vector V_R and the zero lift line of the blade airfoil (radians)
α_c	Angle between the resultant velocity vector V_R and the chord line of the blade airfoil (radians)
δk_Q	Torque loading coefficient of the blade element
δk_T	Thrust loading coefficient of the blade element
η	Efficiency of the propeller
θ_c	Pitch angle of the blade section (radians)
λ	Taper ratio of the propeller blade
ρ	Specific mass of the fluid (air) (kg/m^3)
σ	Solidity of the rotor
ϕ	Angle of the resultant velocity V_R with the plane of rotation of the propeller (radians)

1 Introduction

Small- and medium-sized rotors are used in many recent applications as in propulsion of small airplanes, unmanned aerial vehicles (UAV), autonomous underwater vehicle (AUV), small wind turbines and ducted propellers. Understanding rotor action and interaction with wake flow field are important aspects to better formulate and predict the performance of propeller rotors and wind turbines. Momentum theory applied to rotors and blade element theory were widely used for light loaded blades. Theodorsen [1] developed the propeller theory with ideal load distribution from the dynamics of the wake vortex sheet. This condition of maximum propeller efficiency occurs when the wake vortex sheets are helicoidal without any deformation.

The flow over the rotors is complex due to the interaction between the rotating blades and the wake. For this reason, the precise calculation of the aerodynamic behavior of the rotor depends on the correct modeling of the rotor wake, whose complex nature limits the use of analytical methods, and hence, the numerical methods are inevitably necessary [2].

Dumitrescu and Cardos [2] used a lifting line method to represent the rotor blades with their trailing vortices and

solved the resulting model iteratively. The performance parameters were calculated by the Biot–Savart law and the Kutta–Joukowski theorem.

Palmiter and Katz [3] used a three-dimensional potential flow-based panel code to model the flow over rotating propeller blades, studied the propeller flow problem and validated their predictions with available results.

Slavík [4] presented a procedure for calculating the propeller aerodynamic characteristics with minimum demands on geometrical and aerodynamic propeller input data and propeller blades number.

Gur and Rosen [5] conducted a comparative study among different blade element models for the calculation of the local induced velocity and reported that the blade element momentum model offers good accuracy and high computational efficiency for propeller performance calculations.

Small-scale propeller performance is difficult to predict because of the low Reynolds number and post-stall aerodynamic behavior. Uhlig and Selig [6] investigated the post-stall effects in their experimental work where they tested and analyzed propellers of 6 to 9.9 inches in diameter, two types of taper and settable pitch.

Bohorquez et al. [7] developed a computational method to design and optimize hovering rotors for small-scale vehicles using circular arc airfoils. They presented a detailed experimental investigation on rectangular and tapered blades and implemented a model based on blade element momentum theory. Validation proved that the model can be used to optimize the blade geometry and operating conditions. Khan and Nahon [8] presented a slipstream model based on simple analytical and semiempirical equations and validated their results with experimental data.

XFOIL is a widely used interactive program for the design and analysis of subsonic isolated airfoils. Given the coordinates specifying the shape of a 2D airfoil, Reynolds and Mach numbers, XFOIL can calculate the pressure distribution on the airfoil and hence lift and drag characteristics. The program also allows *inverse design*—it will vary an airfoil shape to achieve the desired parameter [9].

JBLADE is an open-source propeller design and analysis code. The airfoil performance figures needed for the blades simulation come from QBLADE's coupling with the open-source code XFOIL. This integration, which is also being improved, allows the fast design of custom airfoils and computation of their polars. JBLADE uses the classical blade element momentum (BEM) theory modified to account for the 3D flow equilibrium. The code can estimate the performance curves of a given propeller design for off-design analysis [10, 11].

Morgado et al. [12] used the software JBLADE and coupled the BEM formulation and XFOIL. They concluded

that the approach based on the concept of maximum $L^{3/2}/D$ generated more thrust than the concept of maximum L/D .

MacNeill and Verstraete [13] proposed a blade element momentum theory to model low Reynolds number propeller performance and reported significant improvement in accuracy at low advance ratios.

The objective of this study is to conduct a parametric investigation on the Joukowski and Göttingen airfoils for possible use in propellers for small applications. In this study, a validated home-built FORTRAN code based on the **BEM method with incorporated tip, hub and compressibility losses is used. The influences of the airfoil section, chord (linear, constant and elliptic) and pitch angle (linear and constant) distributions including the use of multiple airfoils along the blade are assessed in order to be able to select the best configuration that is efficient and easy to manufacture.** This is done in order to be able to select the best configuration that is efficient and easy to manufacture.

2 Formulation

The propeller develops an axial force called thrust T at an advance velocity V for a rotational speed n due to a torque Q . In this manner, the propeller efficiency is the ratio of the useful power to the power input P

$$\eta = TV / (2\pi n Q) \quad (1)$$

The aerodynamic characteristics are usually expressed in dimensionless forms which depend on the Reynolds and Mach numbers based on the blade tip velocity and the advance ratio J . The advance ratio is defined as

$$J = V / (nD) \quad (2)$$

while the tip velocity is given by

$$V_{\text{tip}} = \pi n D \quad (3)$$

The thrust k_T , torque k_Q and the power k_P coefficients are defined as

$$k_T = T / (\rho n^2 D^4) \quad (4)$$

$$k_Q = Q / (\rho n^2 D^5) \quad (5)$$

$$k_P = P / (\rho n^3 D^5) = 2\pi k_Q \quad (6)$$

In terms of these coefficients, the efficiency of the propeller can be alternatively written as

$$\eta = J k_T / k_P \quad (7)$$

As mentioned before, the calculation routine to predict the general performance of the propeller associates the

momentum theory due to Rankine and Froude [14] with Glauert blade element theory [15]. The Froude momentum theory treats the propeller as a disk with an axial velocity in relation to the disk given by the advance velocity V corrected by the inflow factor a ,

$$V_0 = V(1 + a) \quad (8)$$

From the linear momentum conservation and the pressure difference across the disk, the velocity component well behind the disk V_S is

$$V_S = V(1 + 2a) \quad (9)$$

Glauert's blade element theory for propellers indicates that the velocity component in the plane of rotation V_w can be calculated from

$$V_w = 2\pi n(1 - b)r \quad (10)$$

where b is the swirl factor which accounts for the effects of the wake vortex system on the flow angular velocity in the rotor plane.

Applying the principle of conservation of linear momentum to the flow in an infinitesimal radial ring, one can determine the elementary thrust as

$$dT = 4\pi \rho r V^2 a(1 + a) dr \quad (11)$$

Similarly, the elementary torque is given by

$$dQ = 4\pi \rho r^3 V b(1 + a) 2\pi n d r \quad (12)$$

The elementary thrust and torque can be obtained alternatively from the lift and drag acting on the blade element as below

$$dT = Bc \frac{1}{2} \rho V_R^2 (C_l \cos \phi - C_d \sin \phi) dr \quad (13)$$

$$dQ = Bcr \frac{1}{2} \rho V_R^2 (C_l \sin \phi + C_d \cos \phi) dr \quad (14)$$

where B is the number of blades, V_R is the resultant velocity with reference to the blade and ϕ is the angle of the vector V_R with the plane of rotation of the propeller, as proposed by Houghton et al. [16].

The local resultant velocity V_R is given by

$$V_R = V_0 / \sin \phi = V_w / \cos \phi \quad (15)$$

while the angle ϕ is calculated from

$$\phi = \tan^{-1} \left[\frac{V_0}{V_w} \right] = \tan^{-1} \left[\frac{J}{2\pi(r/D)} \left(\frac{1+a}{1-b} \right) \right] \quad (16)$$

The angle of attack α_c is the angle between the resultant velocity V_R and the chord, calculated as the difference between the pitch angle (twist) of the blade section θ_c and the angle ϕ of the resultant velocity (Fig. 1). The pitch angle θ_c is defined as the angle between the local chord and the plane of rotation of the propeller. The geometric pitch p

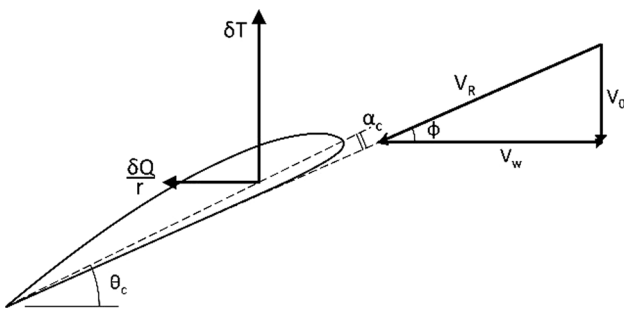


Fig. 1 Cross section of the rotor blade at radius r indicating the velocity components and the acting forces

of the blade section is related to the pitch angle θ_c by the expression $p = 2\pi r \tan \theta_c$.

The geometry of the blade is usually given by the distributions of chord, thickness and the geometrical pitch as function of radius. The pitch angle of the blade is defined as the pitch angle of the blade section localized at $r = 0.75R$ where R is the radius of the blade tip, $R = D/2$.

The tip vortices originating from the extremities of the blade due to the pressure difference at the tip create multiple helical structures in the wake and affect the induced velocity distribution along the propeller effectively reducing the resulting forces in the vicinity of the tip. To correct this deficiency in BEM theory, a tip loss factor, F , originally developed by Prandtl is used, as proposed by Wald [17],

$$F = \frac{2}{\pi} \arccos e^{-f} \quad (17)$$

where

$$f_{\text{tip}} = \frac{B}{2} \frac{R-r}{r \sin \phi} \quad (18)$$

Similarly, the hub loss model serves to correct the induced velocity resulting from a vortex being shed near the hub of the propeller and can be expressed as

$$f_{\text{hub}} = \frac{B}{2} \frac{r-R_{\text{hub}}}{r \sin \phi} \quad (19)$$

For a given element, the local aerodynamics may be affected by both the tip loss and hub loss, in which case the two correction factors are multiplied to create the total loss factor.

The Prandtl loss factor F represents approximately the losses which arise due to the finite number of the propeller blades and should be applied to the propeller theory by the corrected form of the axial momentum equation, Eq. (11), as follows, as proposed by Glauert [18],

$$dT = 4\pi \rho r V^2 a(1+a) F dr \quad (20)$$

Similarly also the angular momentum equation, Eq. (12), may be assumed to be [18]

$$dQ = 4\pi \rho r^3 V b(1+a) 2\pi n F dr \quad (21)$$

The expressions for the elements of thrust and torque in terms of the aerodynamic forces on the blade sections remain unaltered [18]. Equating Eq. (20) to Eq. (13) and Eq. (21) to Eq. (14), one can obtain

$$a = (1/F)(1+a) \frac{\sigma}{4 \sin^2 \phi} (C_l \cos \phi - C_d \sin \phi) \quad (22)$$

$$b = (1/F)(1+a) \frac{\sigma}{4 \sin^2 \phi} (C_l \sin \phi + C_d \cos \phi) \frac{J}{2\pi(r/D)} \quad (23)$$

where σ is the solidity defined as $\sigma = (Bc)/(2\pi r)$.

Equations (22) and (23) can be used to calculate the factors a and b iteratively.

The thrust loading coefficient δk_T of the blade element δr at r is given by

$$\delta k_T = \frac{\frac{dT}{dr}}{B \rho n^2 D^4} \delta r = F \frac{1}{2} c \left[\frac{J(1+a)}{D \sin \phi} \right]^2 (C_l \cos \phi - C_d \sin \phi) \delta r \quad (24)$$

while the torque loading coefficient of the blade δk_Q is given by

$$\delta k_Q = \frac{\frac{dQ}{dr}}{B \rho n^2 D^5} \delta r = F \frac{1}{2} c \left[\frac{J(1+a)}{D \sin \phi} \right]^2 (C_l \sin \phi + C_d \cos \phi) \frac{r}{D} \delta r \quad (25)$$

The coefficients of thrust k_T and torque k_Q of the propeller can be obtained by integrating Eqs. (24) and (25) from the root of the blade to the tip and then multiplying the result by the number of blades B .

One can see that the radial and torque loading coefficients of the blade δk_T and δk_Q depend on the airfoil geometry, its aerodynamic characteristics and the advance ratio J . This also applies to the coefficients of thrust k_T , torque k_Q and power k_P of the propeller.

The specification of the value of the advance velocity V or the rotational speed n determines the Reynolds number of the propeller Re_{75} and allows calculation the global values of thrust T , torque Q and power P . The calculations can be repeated for new values of C_l and C_d coefficients of the local blade chord of the airfoil section, according to the local Reynolds number.

The present numerical code uses expressions to calculate the aerodynamic coefficients of the airfoil section of the blade that were obtained from data of the XFOIL for incompressible flow, so it is necessary to correct for the effects of compressibility, according to the local Mach number of the flow, by the employment of the Prandtl–Glauert correction.

In fact, the portions of the blade near the tip may achieve Mach numbers large enough for the effects of compressibility to become important. Provided that the Mach number of the relative flow does not exceed about 0.70, the effect of compressibility on section drag is very small, but the effect on the lift curve slope may be approximated by the Prandtl–Glauert correction, which states that if the lift curve slope at zero Mach number (i.e., in incompressible flow) is a_0 , the lift curve slope at a subsonic Mach number M is a_M [16], where

$$a_M = \frac{a_0}{\sqrt{1 - M^2}} \quad (26)$$

The procedure adopted in this study to dimension a propeller and evaluate its performance parameters is presented in the block diagram in Fig. 2. Initially, one must define the fluid properties, the rotor geometry (radius and number of blades), blade geometry (chord and twist angle distributions) and the airfoil section aerodynamic characteristics. With these definitions made, one has to divide the blade into N_R radial blade elements where the radius r_i is localized at the center of the element δr . It is calculated the axial induction factor a and tangential b , iteratively. Also the inflow angle and local angle of attack are calculated, and the corresponding aerodynamic coefficients of the airfoil section are obtained from XFOIL for the local Reynolds number range for each iteration. Once the final values of a and b are obtained for a tolerance of 10^{-5} , the thrust and torque loading coefficients of the blade and the coefficients of thrust, torque and power of the propeller are calculated, as well as the total thrust, torque and power values of the propeller.

The number of blade elements N_R used in the calculation affects the distributions along the blade length of the gradient of the thrust coefficient dk_T/dr and also the thrust loading coefficient δk_T . To optimize the number of elements (segments), numerical trials were done using the Clark-Y 5868-9 propeller with 2 blades and with 16, 32 and 48 elements along the blade. The results showed that the variations are very small; we chose $N_R = 16$ because of the small computational time.

3 Validation

To establish the validity of the computational procedure and its viability for calculating the propeller performance, the numerical predictions from the present code are compared with experimental results from Hartman and Biermann [19] and the numerical predictions based on panel method from Palmriter and Katz [3]. The available

experimental results are for the propeller Clark-Y 5868-9, with airfoil Clark-Y, 3.048 m diameter, two blades and for two blade pitch angles of 25° and 35° [19]. The present code uses the data available in Lyon et al. [20] for the aerodynamic coefficients C_l and C_d of the Clark-Y airfoil section for Reynolds number of 3.0×10^5 .

The aerodynamic characteristics of Göttingen 796 were determined from XFOIL [9] for incompressible flow in terms of the Reynolds number and the angle of attack for increments of 0.25°.

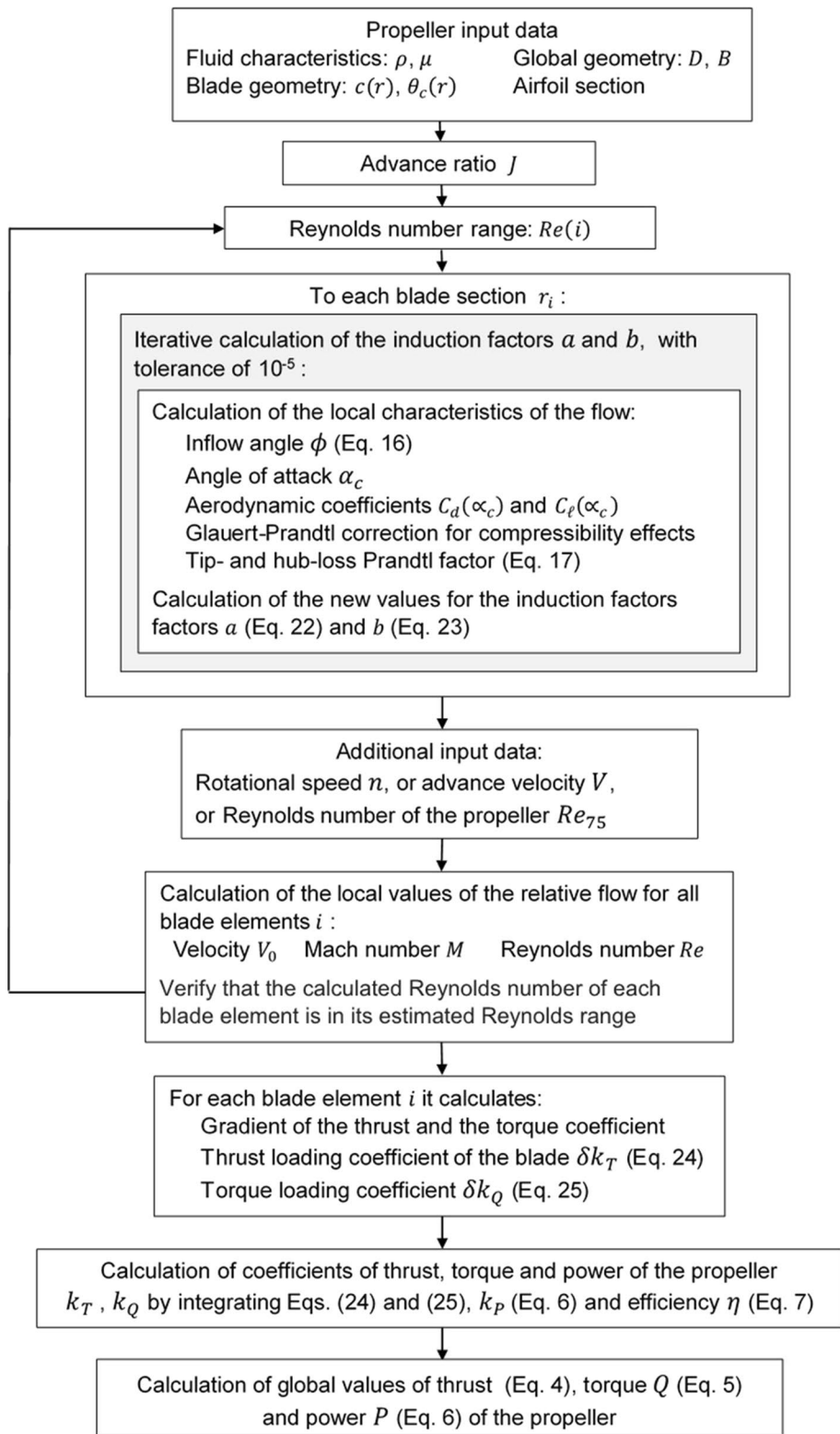
The generalized Joukowski airfoils generated in this study by using the conformal transformation have general characteristics similar to those of Göttingen 796. The aerodynamic coefficients are obtained from XFOIL for the angle of attack and the Reynolds number corresponding to the local blade element.

3.1 Comparison with the experimental and numerical results of the reference propeller

In order to validate the numerical procedure and the code, the coefficients of thrust k_T , power k_p and efficiency η of the propeller predicted from the present code are compared with the experimental results [19] and with the numerical predictions calculated by the panel method [3]. Figure 3a shows the variation in the thrust coefficient with the advance ratio for propeller Clark-Y 5868-9 with pitch angle of 25° at $r/R = 0.75$. This figure shows the experimental results [19], the numerical results from [3], the present results without any correction, the present results corrected for tip and hub effects as well as compressibility effects. As can be verified, all numerical predictions from Palmriter and Katz [3] and from the present code have the same trends and agree reasonably good with the experiments. One can observe that correcting only tip and compressibility effects produces results more close to the experiments and to the panel method predictions. Similar results are found in the case of the coefficient of power shown in Fig. 3b. The inclusion of the hub interference effect based on the available formulation in the literature seems to penalize severely the rotor and reduce its output. A recent review realized shows that this problem is not completely sorted out and needs more analysis and more experimental measurements to quantify better the hub effects. In the present analysis, only the tip and compressibility effects are accounted for. Hence, when referring to Prandtl corrections it means the inclusion of only these two effects.

Both the panel method due to Palmriter and Katz [3] and the present method with and without the inclusion of Prandtl corrections are used to calculate the blade loading as shown in Fig. 4 for the case of pitch angle of 25°. As can be seen, the loading curves follow the same tendencies, but the present method with Prandtl corrections shows higher values

Fig. 2 Block diagram of the propeller calculation procedure



in the region of about 60% to about 90% of the rotor radius compared to the panel method. This effect can be attributed to the correction effects of the tip and compressibility. The

results from the present code show that the inclusion of the Prandtl corrections provides an unloading of the blade tip.

Figure 5a shows a comparison of coefficient of thrust k_T predicted from the present method compared with the

Fig. 3 Effects of the tip, hub and compressibility corrections on the propeller Clark-Y 5868-9, **a** thrust coefficient, **b** power coefficient

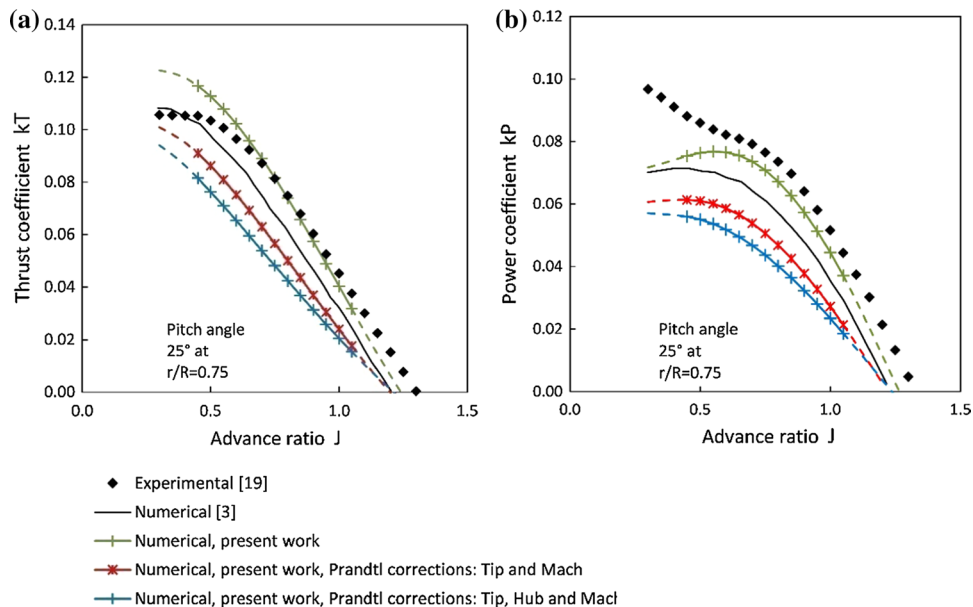
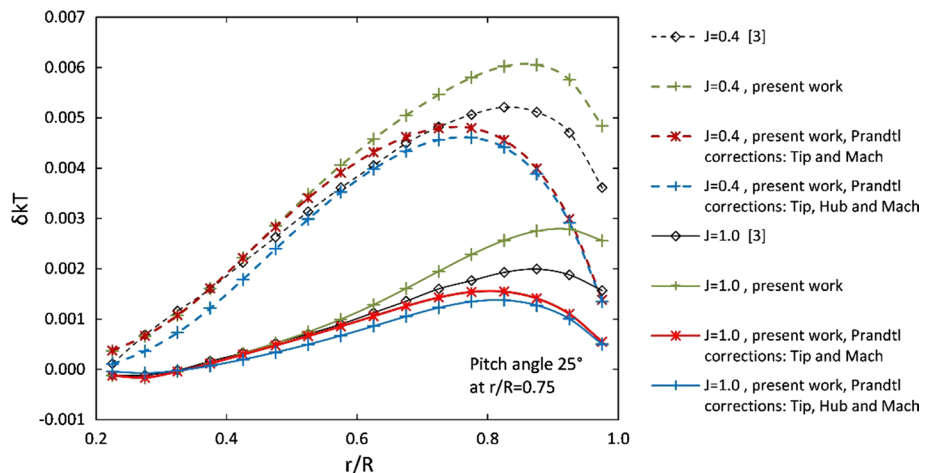


Fig. 4 Comparison between the present predictions of the radial loading along the blade and Palmriter's and Katz [3]

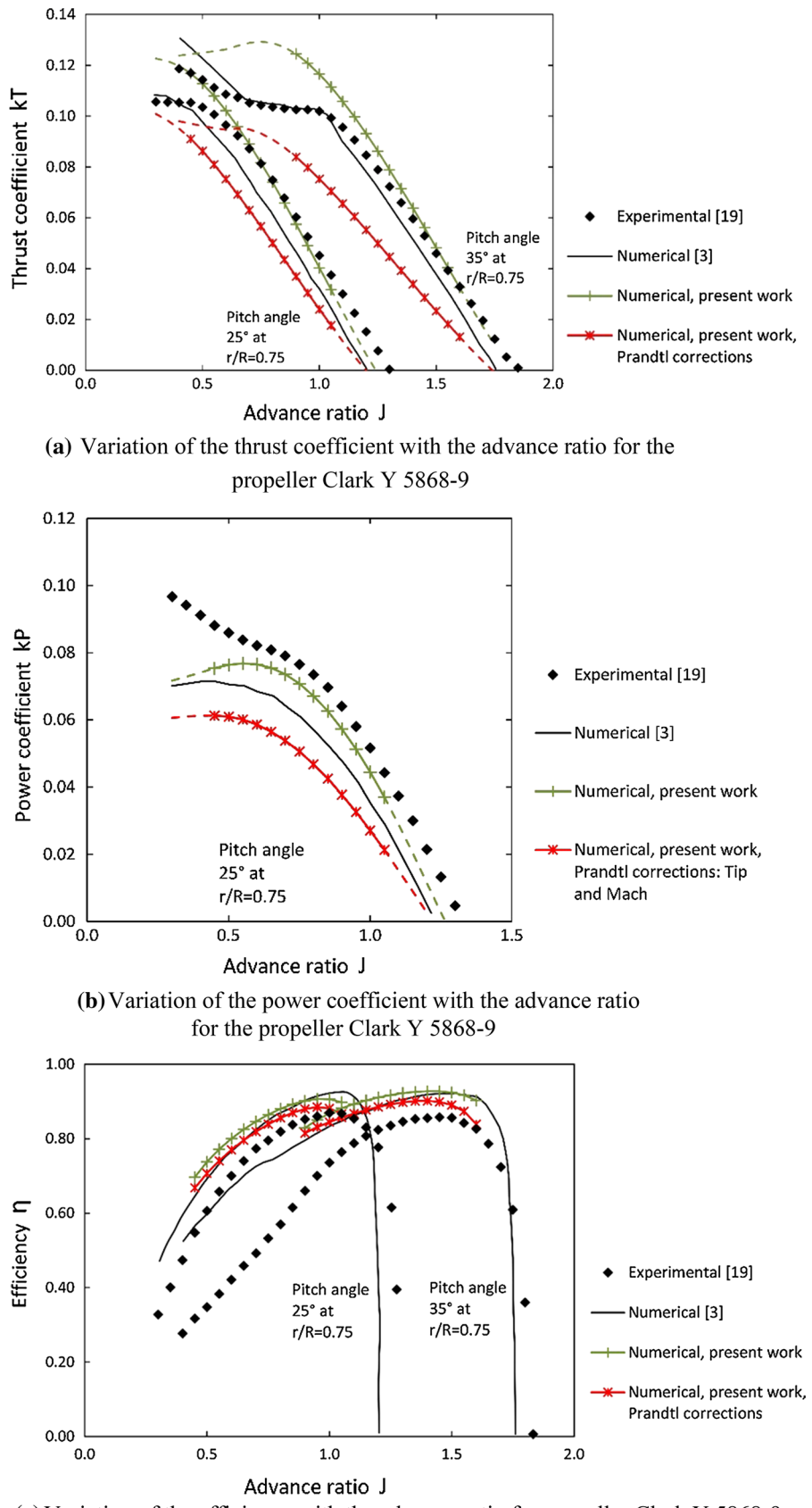


experimental results [19] and with the numerical predictions calculated by the panel method [3]. As can be seen, the agreement is good for the case of pitch angle of 25°. When the pitch angle is increased to 35°, there is a noticeable divergence between the present predictions and the experimental results for low advance ratios due to possible flow separation as mentioned in [3]. To investigate this divergence, the angle of attack is calculated for low advance ratios and for the pitch angles of 25° and 35° at section 0.75R as presented in Fig. 6. Figure 6a shows that for low advance ratio the calculated angle of attack can achieve values as high as 14° for which the airfoil is about to stall or stalling. Examining Fig. 6b shows that for pitch angle of 35° and at low values of advance ratio the calculated angle of attack is about 24°, indicating that the airfoil is operating in stalled conditions. This is in agreement with Palmriter and Katz [3].

Figure 5b shows a comparison between the present predicted values of the coefficient of power k_p , the experimental results from [19] and the numerical predictions based on panel method [3]. One can observe that the numerical predictions from the panel method and the present code have the same tendencies as the experimental results but underestimate the power coefficient. The results from the present code show that the inclusion of the Prandtl corrections unloads the blade tip and reduces the power coefficient.

Figure 5c shows the efficiency of the propeller predicted from the present method and compares the experimental results [19] and numerical predictions [3]. As can be seen, the experimental results agree well with the results of panel method. However, both numerical methods from the present work and from Palmriter and Katz [3] overestimate the efficiency.

Fig. 5 Variation in the thrust coefficient (a), power coefficient (b), efficiency (c) with the advance ratio for the propeller Clark-Y 5868-9



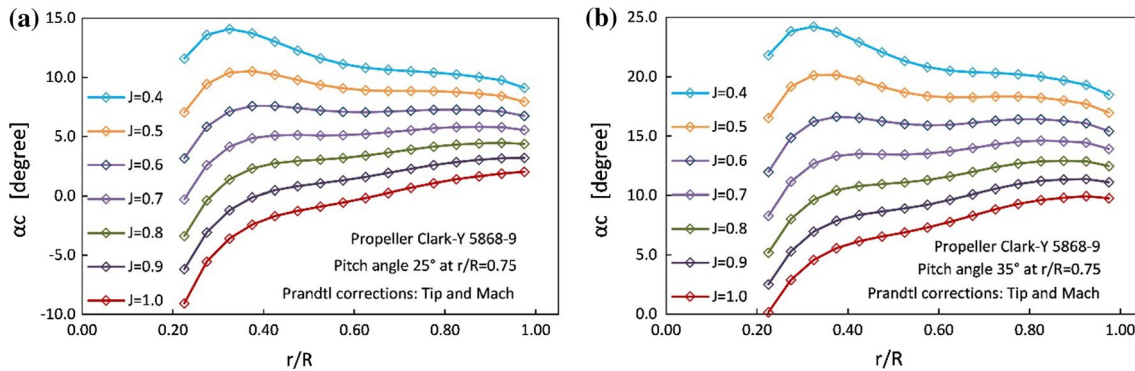


Fig. 6 Variation in the angle of attack for the propeller Clark-Y 5868-9 at low advance ratios for **a** pitch angle 25° and **b** pitch angle 35°

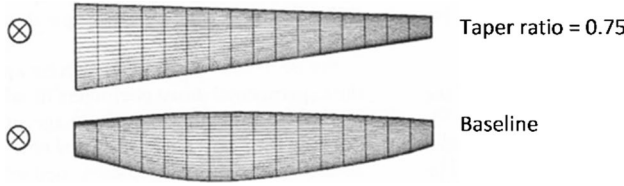


Fig. 7 Comparison of the propeller tapered blade with the blade of the reference propeller [3]

It is interesting to observe that around the advance ratio for best efficiency, that is, around $J=0.95$ ($\eta=0.91$) for the case of pitch angle of 25° and around $J=1.4$ ($\eta=0.94$) for the pitch angle of 35°, the present predicted results are better for both coefficients k_T and k_P as shown in Figs. 3 and 4.

3.2 Comparison with the blade proposed by [3]

The proposed propeller [3] has a diameter of 10 ft and trapezoidal blade based on airfoil Clark-Y of thickness varying linearly between 20% at the root and 9% at the tip of the blade. The pitch angle of the sections changes linearly from the root to the tip and is defined as that of the radial section at $r=0.75R$. The taper ratio, defined as the ratio of the tip chord/root chord, considered for comparison is 0.75, as shown in Fig. 7 reproduced from [3].

The present authors used this information to calculate the blade loading with taper ratio 0.75 and pitch angle of 25° and compared the predictions with those due to Palmeter and Katz [3], as shown in Fig. 8. As can be seen, the predicted results seem to agree well until $r=0.75R$ after which it slightly overestimates the loading. With the increase in the advance ratio, the differences between the present results and those of Palmeter and Katz [3] are reduced and better agreement is obtained as shown in Fig. 8 for the case (c).

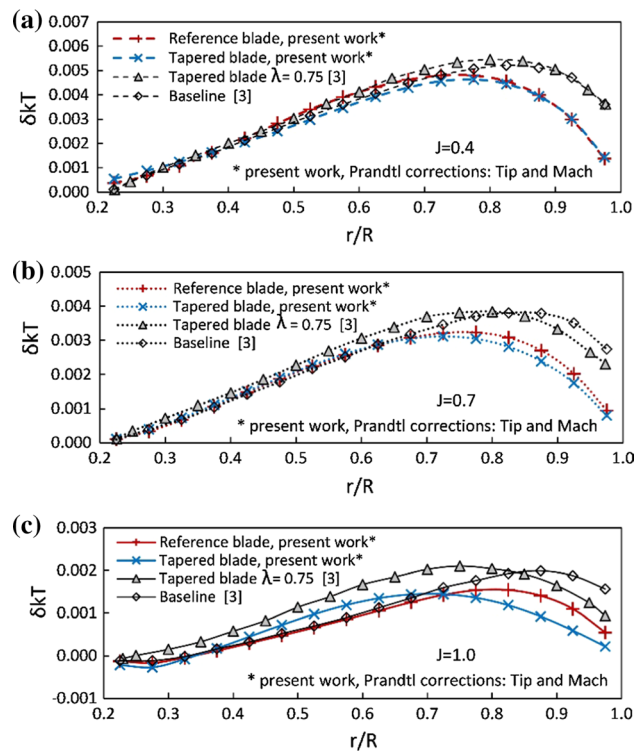


Fig. 8 Comparison of the radial loadings along the reference blade and the tapered blade ($\lambda=0.75$)

One can observe, as shown in Fig. 8, that the present predicted results indicate that the tip region of the modified propeller is less loaded (except for $J=0.4$) in comparison with the blade of the reference propeller, and that the loading is heavier in the central region of the blade. These effects are intensified with the increase in the advance ratio and agree and have the same tendencies as in [3].

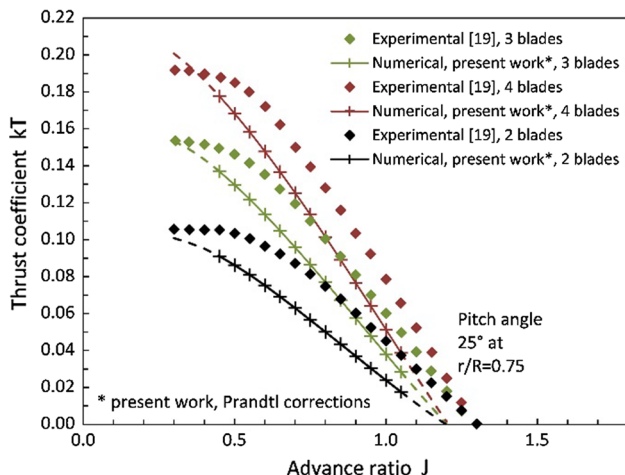


Fig. 9 Comparison of the thrust coefficient of the Clark-Y 5868-9 propeller with the experiments [19] for 2, 3 and 4 blades

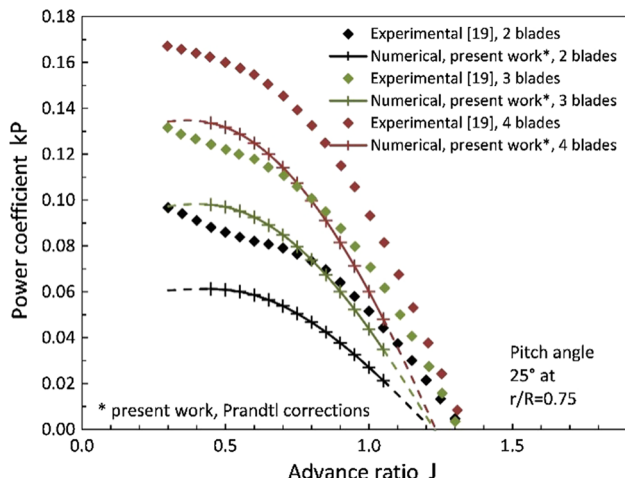


Fig. 10 Comparison of the power coefficient of the Clark-Y 5868-9 propeller with the experiments [19] for 2, 3 and 4 blades

3.3 Comparison with the reference propeller (different number of blades)

The experimental results of the thrust and power coefficients from Hartman and Biermann [19] for different number of blades are used for comparison with the present numerical predictions under the same working conditions with the Prandtl corrections included in the numerical code. One can observe that the present numerical method agrees well the experimental data as the number of blades increases. The thrust and power coefficients of the propeller increase as the number of blades increases, as shown in Figs. 9 and 10, respectively. However, the present numerical method underestimates the power coefficient mainly for the case of two blades.

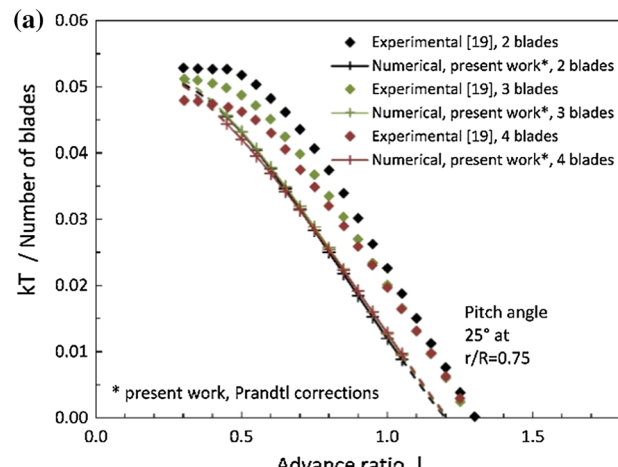


Fig. 11 Comparison of the thrust coefficient by number of blades of the Clark-Y 5868-9 propeller with the experiments of [19] for 2, 3 and 4 blades, **a** thrust coefficient by number of blades, **b** the power coefficient by number of blades and **c** efficiency

However, as an alternative way to investigate the influence of the number of blades on the thrust and the power coefficients, one can plot the thrust and the power

coefficients divided by the number of blades as shown in Figs. 11. Inspecting this figure, one can observe that the thrust coefficient varies marginally. Figure 11b shows that the increase in the number of blades produces decreasing effect on the power coefficient. The increase in the number of blades leads to the increase in the inflow velocity, i.e., the axial component of the flow velocity relative to the blade in the rotor plane, for the same advance velocity of the rotor. In this way, the results of the coefficients of thrust and power show small increase with the increase in the number of blades. This is in agreement with Hartman and Biermann [19] conclusions.

The tendency of the efficiency of the propeller follows the same trends as in the experiments and decreases as the number of blades increases as shown in Fig. 11c. The results of efficiency obtained in the present work show a decrease with the increase in the number of blades. The experimental results show that in the region where the blades start to stall because of the smaller advance ratio, the efficiency of the rotors with 3 and 4 blades tends to increase.

This can be explained by the fact that the higher inflow velocities for rotors of 3 and 4 blades reduce the stall effects which is in agreement with Hartman and Biermann [19].

4 Results and discussion

The reference propeller used here for comparison is a propeller based on the airfoil Clark-Y 5868-9 whose geometry and experimental results were presented in [19]. The rotor has two blades, 3.048 m diameter and pitch of 25°. The present code uses the data for airfoil Clark-Y available in Lyon et al. [20] for Reynolds number of 3.0×10^5 .

The validated code was used to calculate a propeller with the airfoil Göttingen 796 similar to the original airfoil

Clark-Y but has a higher value of the ratio C_t/C_d . The characteristics of Göttingen 796 were determined from XFOIL [9] for incompressible flow with Reynolds numbers of 0.50×10^6 , 0.75×10^6 , 1.00×10^6 , 1.25×10^6 , 1.50×10^6 , 1.75×10^6 and 2.00×10^6 . The curves of the lift and drag coefficients were obtained in terms of the angle of attack for increments of 0.25° and incorporated in the numerical code.

To investigate the effect of airfoil section, two families of airfoils were selected, that is, Göttingen and Joukowski. The traditional Joukowski airfoil has a cusped trailing edge which makes it unsuitable for the present application. Glauert [21] presented a method to obtain generalized airfoils more suitable for the practical use by using the conformal transformation $[(\zeta - nc)/(\zeta + nc)] = [(z - c)/(z + c)]^n$. Details of this transformation can be found in [21]. The generalized Joukowski J 12 3.8 .25 generated for this study has general characteristics similar to those of Göttingen 796 as shown in Table 1 and Fig. 12.

All results presented in this section have been corrected for tip and compressibility effects.

Propeller G1 is a Göttingen 796-based propeller that has exactly the same geometry and operational conditions as the reference propeller. Figure 13a shows the predicted thrust and power coefficients and efficiency of the propeller G1 compared with those of the reference propeller. As can be seen, the propeller G1 shows higher values due to the differences in the aerodynamic characteristics of the two airfoils.

Figure 13b shows the spanwise distribution of blade loading for both propellers for the advance ratio $J = 1$ corresponding to maximum efficiency. The root region is defined between $r/R = 20\%$ and $r/R = 40\%$, while the tip region is defined between $r/R = 80\%$ and the blade tip. The respective local contributions of the three regions of propeller G1 to the total thrust are: –2.2% for root region, 64.1% for the intermediate region and 38.1% for the tip

Table 1 Characteristics of Göttingen and generalized Joukowski airfoils

Airfoil section	Maximum thickness/chord (%)	Maximum camber/chord (%)	Trailing edge angle (radians)
Göttingen 796	12.0 at 30% chord	3.6 at 40% chord	–
Joukowski J 12 3.8 .25 ($k = 1.060$, $\beta = 4.5^\circ$, $n = 1.920$)	12.3 at 36.8% chord	3.8 at 51.8% chord	0.2513

Fig. 12 Göttingen 796 and the generalized Joukowski J 12 3.8 .25 airfoils



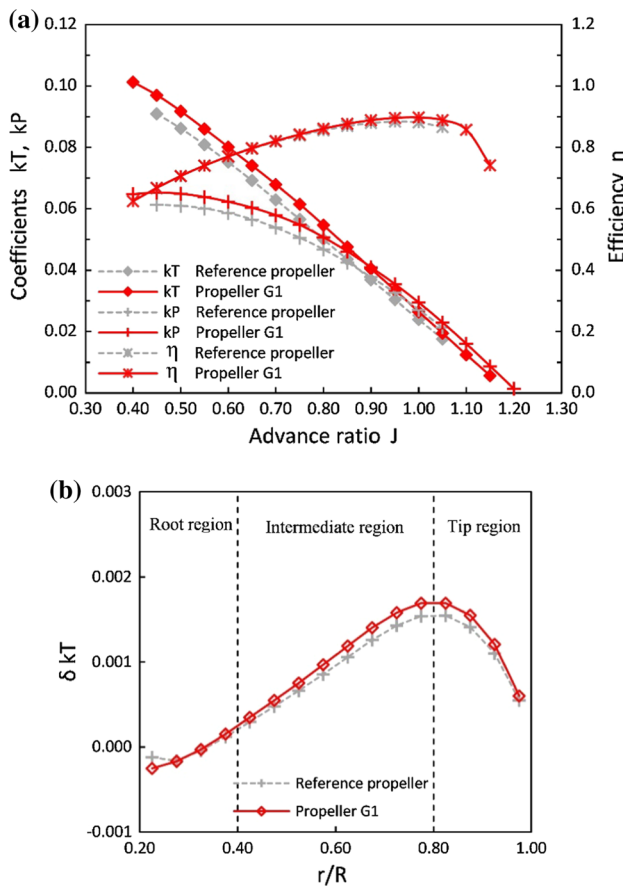


Fig. 13 Comparison of the characteristics of the propeller based on Göttingen 796 and the reference propeller, **a** aerodynamic coefficients, **b** distribution of the thrust loading for advance ratio $J = 1.0$

region. In the case of the reference propeller, the contributions are: – 1.8% for root region, 63.3% for the intermediate region and 38.5% for the tip region.

Propeller J1 is a Joukowski-based propeller that has exactly the same geometry and operational conditions as the reference propeller, except that the airfoil section is the generalized Joukowski J 12 3.8 .25 airfoil, see Table 1.

Figure 14a shows a comparison between the predicted thrust and power coefficients and efficiency of the propeller J1 and the reference propeller. As can be seen, the propeller J1 shows higher values due to the differences in the aerodynamic characteristics of the two airfoils, and the differences in the respective coefficients increase as the advance ratio increases.

Figure 14b shows the spanwise distribution of blade loading for both propellers for the advance ratio $J = 1$ corresponding to maximum efficiency. The respective local contributions of the three regions of propeller J1 to the total thrust are: 0.4% for root region, 64.6% for the intermediate region and 35.0% for the tip region. In the case

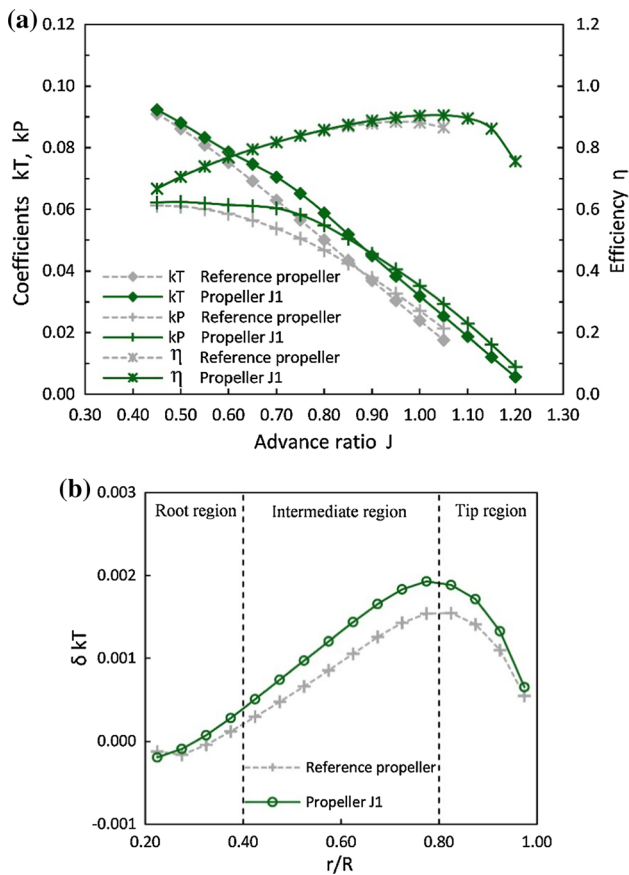


Fig. 14 Comparison of the propeller based on the Joukowski J 12 3.8 .25 airfoil and the reference propeller, **a** the aerodynamic coefficients, **b** the thrust loading distribution for advance ratio $J = 1.0$

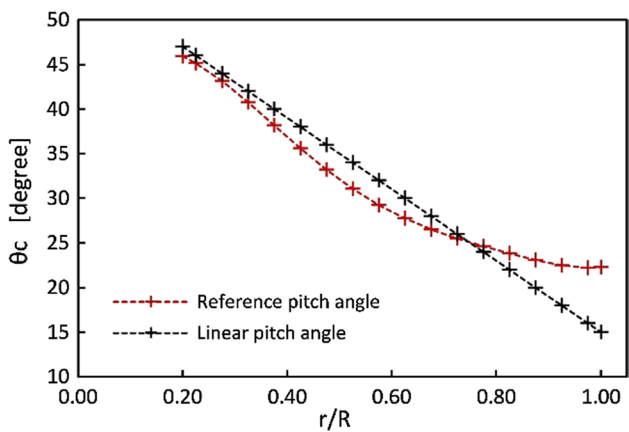


Fig. 15 Comparison of proposed linear pitch angle distribution and reference pitch angle distribution of the reference propeller

of the reference propeller, the contributions are: 1.8% for root region, 63.3% for the intermediate region and 38.5% for the tip region.

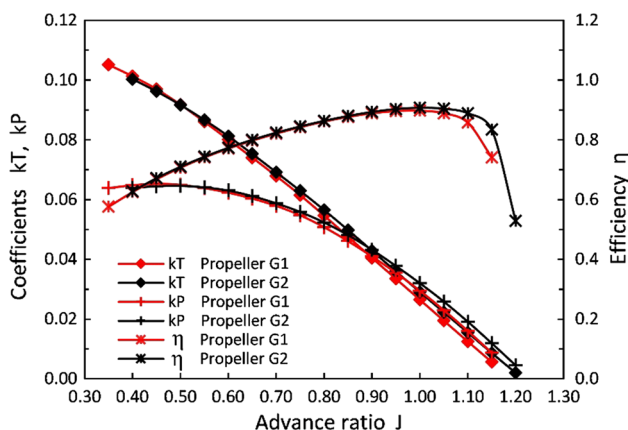


Fig. 16 Comparison of aerodynamic coefficients of propeller G2 with linear pitch distribution and propeller G1 with reference pitch distribution

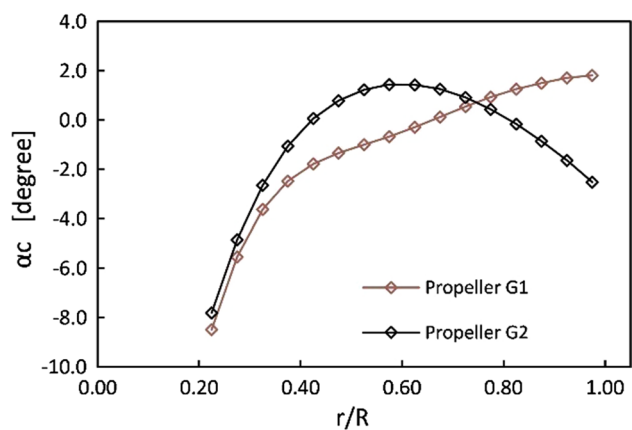


Fig. 18 Comparison of the local angle of attack of the sections of the blade calculated for propellers G1 and G2

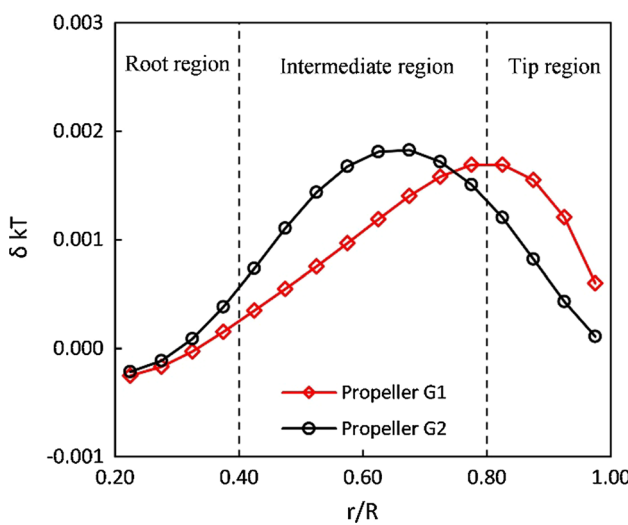


Fig. 17 Comparison of thrust loading distribution of propeller G2 with linear pitch distribution and propeller G1 with reference pitch distribution for advance ratio $J=1.0$

4.1 Distribution of pitch angle

The reference propeller and the propeller G1 have the same reference distribution of pitch angle along the blade as presented in Hartman and Biermann [19] for the Clark-Y 5868-9 propeller, shown in Fig. 15.

Propeller G2 is a Göttingen-based propeller, the same as the propeller G1, except that it has linear pitch angle distribution along the blade, as shown in Fig. 15. We introduce propeller G2 to investigate the effect of the pitch distribution on the performance of the propeller.

Figure 16 shows the predicted results of the thrust and power coefficients as well as the efficiency for the propeller G1 and the propeller G2. One can observe that propeller G2 shows coefficients of thrust and power slightly bigger than propeller G1 but has nearly the same efficiency.

Figure 17 shows that propeller G2 (based on assuming linear distribution of pitch angle) produces higher blade loading at the intermediate region and lower blade loading at the tip region in comparison with propeller G1 (based on the reference distribution as shown in Fig. 15). Also one can observe that the linear distribution of pitch angle favors reduced loading at the tip region which helps in reducing mechanical loads at the root region. The respective local contributions of the three regions of propeller G2 to the total thrust are: 1.0% for root region, 81.3% for the intermediate region and 17.7% for the tip region. In the case of the propeller G1, the contributions are: -2.2% for root region, 64.1% for the intermediate region and 38.1% for the tip region for the tip region.

As shown in Fig. 18, the use of the linear pitch angle distribution of the blade produces bigger local angles of attack in the intermediate blade region and smaller angles in the blade tip region than those produced by the reference distribution of pitch angle.

Similar results were obtained for the Joukowski airfoil and are omitted for the sake of brevity.

4.2 Effect of airfoil section

To investigate the effect of the airfoil section on the aerodynamic performance of the rotor of the propeller, we introduce propeller J2. Propeller J2 is a Joukowski-based propeller with linear pitch distribution and has exactly the same geometry and operational conditions as the propeller G2, except that the airfoil section is the generalized Joukowski J 12 3.8 .25 airfoil.

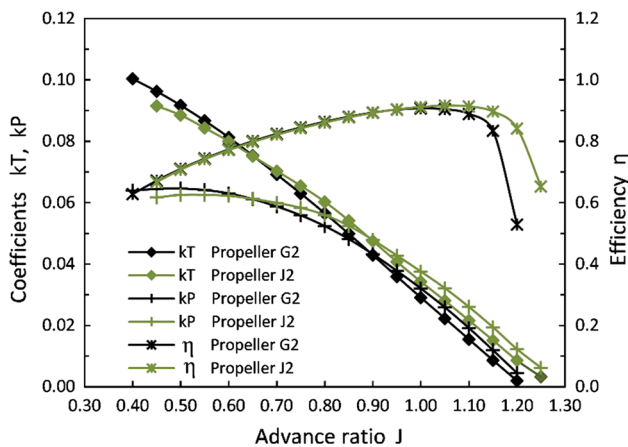


Fig. 19 Comparison of the aerodynamic coefficients of propeller J2 and propeller G2, both with the same reference chord and with linear pitch angle distributions

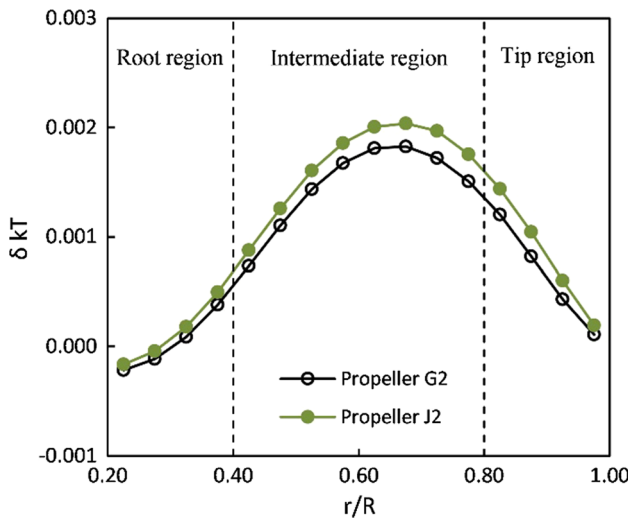


Fig. 20 Comparison of thrust distribution of propeller J2 and propeller G2 for advance ratio $J=1.0$

Figure 19 shows that the thrust and the power coefficients and the efficiency of the propeller J2 are greater than the respective coefficients of propeller G2 for advanced ratio $J=0.65$ or higher while Fig. 20 shows that the blade thrust loading of propeller J2 is higher but shows the same trend as the loading of propeller G2. Both propellers have well-loaded intermediate region and less loaded blade tip region due to the linear pitch angle distribution.

The respective local contributions of the three regions of propeller J2 to the total thrust are: 2.8% for root region, 78.1% for the intermediate region and 19.1% for the tip region. In the case of the propeller G2, the contributions are: 1.0% for root region, 81.3% for the intermediate region and 17.7% for the tip region.

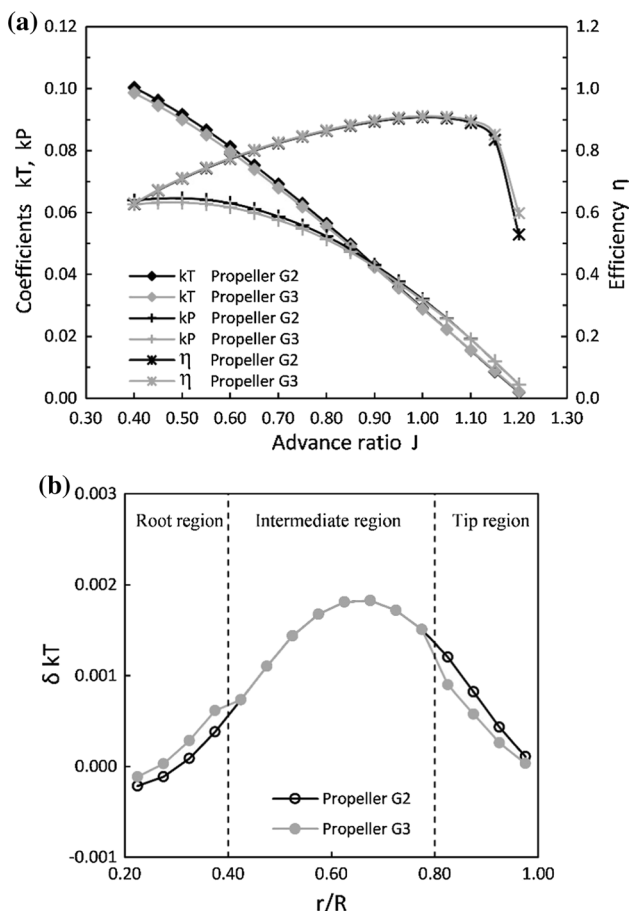


Fig. 21 Comparison of aerodynamic coefficients and loading of the propeller G3 and propeller G2, **a** aerodynamic coefficients, **b** blade loading for advance ratio $J=1.0$

4.3 Effect of multiple airfoil sections along the blade

Effect of multiple airfoils along the blade can be used to change the load distribution according to the aerodynamic project. In order to uniformize the blade loading and reduce its distribution at the tip, we used three different profiles along the blade. For each airfoils family, that is, Göttingen and Joukowski, it is studied the case using three different airfoils of the same family along the blade. As before, the root region is defined between $r/R=20\%$ and $r/R=40\%$, while the tip region is defined between $r/R=80\%$ and the blade tip. For the root region, a thick airfoil was selected because it is adequate for the mechanical fixation of the blades; for the tip region a thin airfoil with small camber was adopted while for the middle region the same airfoil used in the single blade case was used.

Göttingen airfoils family Propeller G3 is a propeller with multi Göttingen airfoils, and it is exactly as propeller G2, except that it has three different airfoil sections along

Table 2 Characteristics of Göttingen airfoil sections

Airfoil section	Maximum thickness/chord (%)	Maximum camber/chord (%)
Göttingen 449	17.0 at 30% chord	5.4 at 40% chord
Göttingen 796	12.0 at 30% chord	3.6 at 40% chord
Göttingen 622	8.0 at 30% chord	2.4 at 40% chord

the blade, where airfoil Göttingen 449 is used for the root region, airfoil Göttingen 796 for the middle part of the blade and airfoil Göttingen 622 for the tip region of the blade.

Figure 21a shows the performance coefficients for the propeller G3 compared to propeller G2. One can observe that the thrust and power coefficients of propeller G3 are smaller than those of propeller G2. The efficiency curve seems to be less affected by using different airfoils along the blade length.

Figure 21b shows the thrust loading coefficient for the propeller G2 with one airfoil along the blade and propeller G3 with three airfoils along the blade. As can be seen, propeller G3 shows bigger loading at the root region and lower loading at the tip region. This is due to the fact that the Göttingen 449 airfoil at the root region has a camber ratio of 5.4% more than that of the Göttingen 796 of 3.5% camber of propeller G2 in the same region. The tip region Göttingen 622 airfoil has a camber ratio of 2.4% that less than that for case of propeller G2. The characteristics of these airfoil sections are shown in Table 2.

The respective contributions of the three regions of propeller G3 with multi Göttingen airfoils to the total thrust are 5.7% for root region, 82.0% for middle region and 12.3% for the tip region, as shown in Table 3.

Joukowski airfoils family Propeller J3 is a generalized Joukowski-based propeller that is exactly the same as

propeller J2, except that it has three different airfoil sections along the blade, where airfoil Joukowski J 17 5.1 .28 is used for the root region, airfoil Joukowski J 12 3.8 .25 for the middle part of the blade and airfoil Joukowski J 8 2.4 .13 for the tip region of the blade, see Table 4 for more details.

Figure 22a shows the performance coefficients for the propeller J3 compared to propeller J2. One can observe that the thrust and power coefficients of propeller J3 are less than those of propeller J2. Multiple airfoils along the blade length seem to have little effect on the efficiency curve.

Figure 22b shows the thrust loading coefficient for the propeller J2 with one airfoil along the blade and propeller J3 with three airfoils along the blade. As can be seen, propeller J3 shows little bigger loading at the root region and lower loading at the tip region. This is due to the fact that the Joukowski J 17 5.1 .28 airfoil at the root region has a camber ratio of 5.1% more than that of the Joukowski J 12 3.8 .25 of 3.8% camber of propeller J2 in the same region. The tip region Joukowski J 8 2.4 .13 airfoil has a camber ratio of 2.4% less than that for case of propeller J2. The characteristics of these airfoil sections are shown in Table 4.

The respective contributions of the three regions of propeller J3 to the total thrust are 5.4% for root region, 82.0% for middle region and 12.6% for the tip region, as shown in Table 5.

The efficiency curves do not show any noticeable variation due to using multiple airfoils along the blade. Also from the predicted results, the propeller with three airfoils along the blades shows bigger loading at the root region and lower loading at the tip than that of the propeller with only single airfoil along the blade which is beneficial from the mechanical strength point of view.

Table 3 Performance characteristics and blade loadings of the propeller G2 with a single Göttingen 796 airfoil along the blade compared with the propeller G3 with three different Göttingen airfoils for $J=1.0$ (The two propellers have reference chord distribution)

Propeller	Airfoil section	Pitch angle	η	T (N)	Q (Nm)	Thrust loading of the blade (%)		
						Root	Intermediate	Tip
Propeller G2	Göttingen 796	Linear	0.9075	853	456	0.97	81.35	17.68
Propeller G3	Göttingen 449 Göttingen 796 Göttingen 622	Linear	0.9115	846	450	5.70	82.03	12.27

Table 4 Characteristics of generalized Joukowski airfoil sections

Airfoil section	Maximum thickness/chord (%)	Maximum camber/chord (%)	Trailing edge angle (radians)
Joukowski J 17 5.1 .28 ($k=1.100$, $\beta=6.0^\circ$, $n=1.910$)	16.9 at 33.6% chord	5.1 at 50.4% chord	0.2827
Joukowski J 12 3.8 .25 ($k=1.060$, $\beta=4.5^\circ$, $n=1.920$)	12.3 at 36.8% chord	3.8 at 51.8% chord	0.2513
Joukowski J 8 2.4 .13 ($k=1.045$, $\beta=2.8^\circ$, $n=1.960$)	8.0 at 33.3% chord	2.4 at 50.7% chord	0.1257

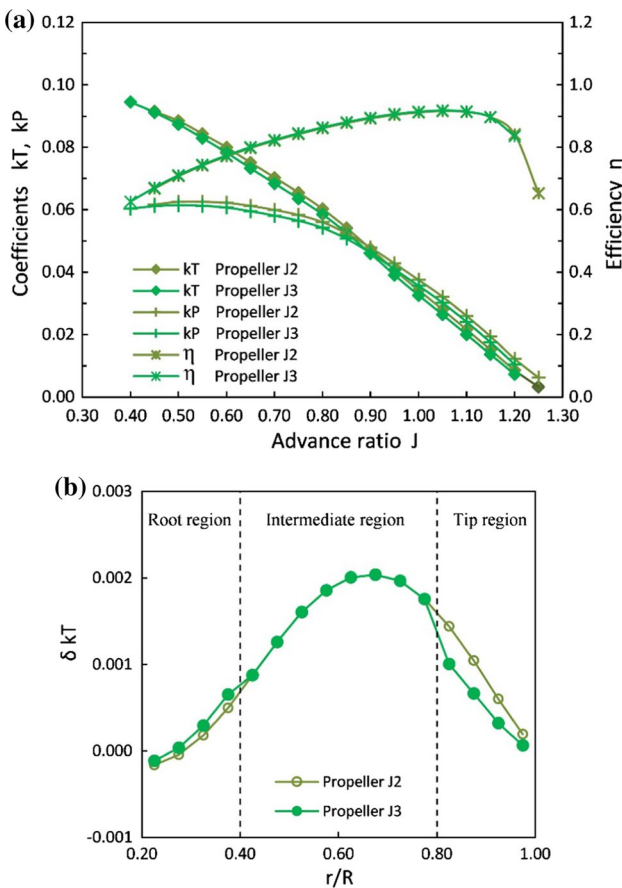


Fig. 22 Comparison of aerodynamic coefficients and loading of propeller J3 and propeller J2, **a** aerodynamic coefficients, **b** blade loading for advance ratio $J=1.0$

4.4 Effect chord distribution

Further calculations were realized to investigate the effects of chord distribution on the blade loading and on the performance characteristics of the propeller.

4.4.1 Propeller with Göttingen airfoil

In this case, the propellers have exactly the same geometry, same operational conditions, and the same airfoil Göttingen 796 and have linear pitch angle distribution along the

blade, as the propeller G2. The chord length in the middle of the blade is kept equal to the value corresponding to that of the reference propeller at section $r/R=0.75$. The chord distributions adopted for investigation include elliptic chord distribution and chord distributions with taper ratios $\lambda=1.0$, $\lambda=0.75$, $\lambda=0.50$ and $\lambda=0.30$.

Figure 23 shows that tapered blade reduces the local loading at the tip region and increases the blade loading at intermediate region of the blade in comparison with the reference chord distribution. These changes become more noticeable with the increase in the blade taper or the decrease of λ .

One can also observe that the elliptic chord distribution resulted in reduced loading in comparison with the reference chord distribution and the tapered blades. The results for elliptic chord are close to those of the blade with taper ratio of 0.30. Effects of varying the chord distribution for advance ratio $J=1.0$ are shown in Table 6 and Fig. 21.

The numerical predictions show that the reduction in the blade loading at the tip region and its increase in the middle part of the blade can be obtained by adopting linear distribution of the pitch angle or by using tapered blade. These effects are intensified by the increase in the blade taper ratio. It is also possible to observe from the predicted results that the use of the elliptical chord distribution instead of tapered blade accentuates these effects. However, the changes in the geometry of the blade reduce the blade loading near the tip but also reduce the coefficient of thrust, torque and power at nearly constant efficiency, in comparison with the blade having the reference chord distribution. It is obvious that elliptic chord distribution adds more difficulties to the manufacturing process and increases the production costs.

It was observed that the calculation with the Prandtl corrections presents greater loading of the intermediate region and lower loading of the tip region of the blades compared to the calculation without the Prandtl corrections. In the case of the propeller with Göttingen 796 airfoil and blade tapered with $\lambda=0.30$, the loading of the intermediate region changes from 74.7 to 82.9% (thus an increase of +11.0%), the loading of the blade tip region changes from 25.4 to 17.4% (about -31.5%), and there is variation of -27.0% in the thrust and -26.2% in the propeller torque.

Table 5 Performance characteristics and blade loadings of the propeller J2 with a single generalized Joukowski airfoil along the blade compared with the propeller J3 with three different Joukowski airfoils for $J=1.0$. (The two propellers have reference chord distribution)

Propeller	Airfoil section	Pitch angle η	T (N)	Q (Nm)	Thrust loading of the blade (%)		
					Root	Intermediate	Tip
Propeller J2	Joukowski J 12 3.8 .25	Linear	0.9121	1006	535	2.77	78.08
Propeller J3	Joukowski J 17 5.1 .28	Linear	0.9143	958	508	5.35	82.02
	Joukowski J 12 3.8 .25						12.64
	Joukowski J 8 2.4 .13						

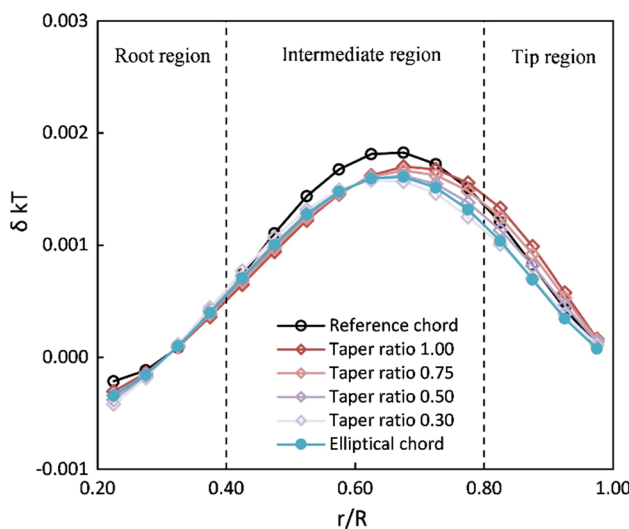


Fig. 23 Comparison of thrust distribution of propellers using airfoil Göttingen 796 and different chord distributions along the blade, for advance ratio $J=1.0$ (all propellers have linear pitch angle distribution)

4.4.2 Propeller with generalized Joukowski airfoil

A similar study is also made for the propellers with generalized Joukowski airfoil section.

The propellers have exactly the same geometry and operational conditions as the propeller J2, with generalized Joukowski J 12 3.8 .25 airfoil and linear pitch angle distribution along the blade, except that the chord distribution is modified. The chord length in the middle of the blade length is

kept equal to the value corresponding to that of the reference propeller at section $r/R=0.75$. The blade loading is calculated for taper ratio $\lambda=1.0$, $\lambda=0.75$, $\lambda=0.50$, $\lambda=0.30$ and for elliptic blade.

Effects of varying the chord distribution for advance ratio $J=1.0$ are shown in Table 7 and Fig. 24. One can observe that the effects of chord distribution on the blade loading and on the performance characteristics of the propeller with Joukowski airfoil are similar to those observed in the case of the propeller with Göttingen airfoil for the same chord distribution along the blade.

As in the previous case, the inclusion of Prandtl corrections results in greater loading of the intermediate region and lower loading of the tip region of the blades compared to the calculation without the Prandtl corrections. For example, in the case of the propeller with Joukowski J 12 3.8 .25 airfoil and blade tapered with $\lambda=0.30$, the loading of the intermediate region changes from 69.9 to 78.4% (thus an increase of +12.2%), the loading of the blade tip region changes from 27.8% to 18.7% (about -32.7%), and there is variation of -27.7% in the thrust and -26.2% in the propeller torque.

4.5 Effect of number of blades

In Sect. 3.3, the numerical code was validated with the experimental results of Hartman and Biermann [19] for Clark-Y 5868-9 reference propeller with 2, 3 and 4 blades. Additional verification of the effect of the number of blades is done by calculating the propeller J2, with generalized Joukowski J 12 3.8 .25 airfoil, reference chord and linear

Table 6 Performance characteristics and blade loadings of the propellers with Göttingen 796 airfoil and different chord distributions on the blade for $J=1.0$ (linear pitch angle distribution)

Chord	η	T (N)	Q (Nm)	Thrust loading of the blade (%)		
				Root	Intermediate	Tip
Reference	0.9075	853	456	0.97	81.35	17.68
Straight, $\lambda=1.00$	0.9056	816	437	0.10	77.88	22.02
Tapered, $\lambda=0.75$	0.9069	799	427	-0.03	79.05	20.98
Tapered, $\lambda=0.50$	0.9083	774	413	-0.18	80.78	19.41
Tapered, $\lambda=0.30$	0.9095	744	397	-0.34	82.91	17.43
Elliptic	0.9120	743	395	0.02	82.94	17.03

Table 7 Performance characteristics and blade loadings of the propellers with generalized Joukowski airfoil and different chord distributions on the blade for $J=1.0$ (linear pitch angle distribution)

Chord	η	T (N)	Q (Nm)	Thrust loading of the blade (%)		
				Root	Intermediate	Tip
Reference	0.9121	1006	535	2.77	78.08	19.15
Straight, $\lambda=1.00$	0.9111	974	519	2.32	73.83	23.85
Tapered, $\lambda=0.75$	0.9128	954	507	2.45	74.86	22.68
Tapered, $\lambda=0.50$	0.9149	924	490	2.66	76.41	20.93
Tapered, $\lambda=0.30$	0.9169	889	470	2.90	78.44	18.67
Elliptic	0.9184	880	465	2.78	79.05	18.17

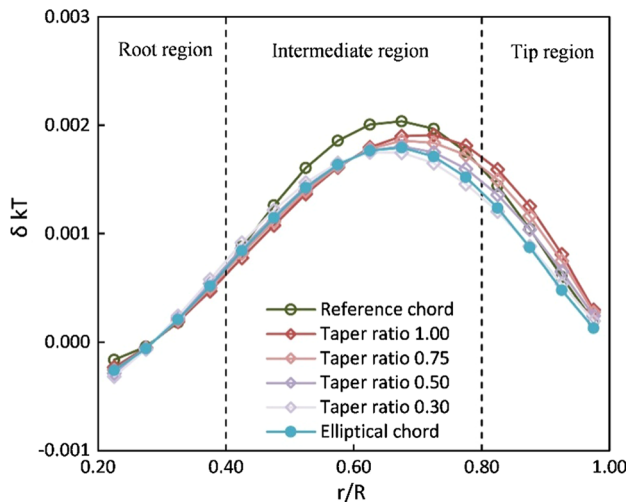


Fig. 24 Comparison of thrust distribution of propellers with generalized Joukowski airfoil for different chord distributions along the blade, for advance ratio $J=1.0$ (all propellers have linear pitch angle distribution)

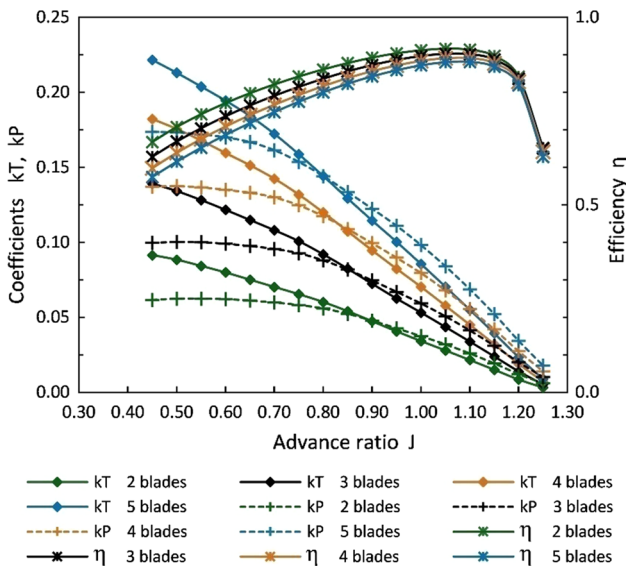


Fig. 25 Comparison of aerodynamic coefficients of propeller J2 (airfoil Joukowski J 12 3.8 .25, reference chord, linear pitch angle) with 2, 3, 4, and 5 blades

pitch angle distributions along the blade and with 2 blades as before and with 3, 4 and 5 blades. The results are shown in Figs. 25 and 26.

Figure 25 shows that the coefficients of thrust and power of the propeller increase and the efficiency of the propeller decreases as the number of blades increases. However, Fig. 26 shows that the coefficient of thrust per blade decreases while the coefficient of power per blade increases as the number of blade increases.

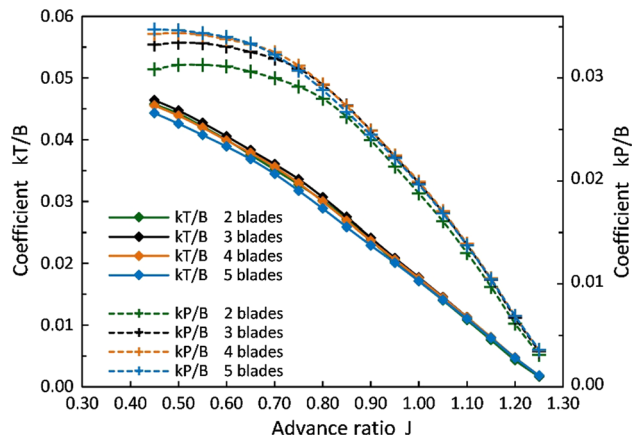


Fig. 26 Comparison of aerodynamic coefficients by blade unit to propeller J2 (airfoil Joukowski J 12 3.8 .25, reference chord, linear pitch angle) with 2, 3, 4, and 5 blades

5 Conclusions

The home-built numerical code based on the momentum theory and blade element theory calculates the performance parameters of the propeller including thrust loading, blade thrust, torque and power coefficients, and efficiency of the propeller as functions of the advance ratio. Predictions from the present method for the reference propeller Clark-Y 5868-9 are in agreement with both experimental results and numerical calculations by the panel method.

The effects of the airfoil section, chord (linear, constant and elliptic), pitch angle (linear and constant) distributions and the use of multiple airfoils along the blade on the aerodynamic characteristics of the propeller are evaluated. This is done in order to enable the selection of the best configuration that is efficient and easy to manufacture and if a compromise solution is to be adopted in favor of the easiness of fabrication the decision maker can estimate the performance cost.

The predicted thrust and power coefficients and efficiency of the propeller G1 showed higher values in comparison with the reference propeller due to the differences in the aerodynamic characteristics of the two airfoils. The spanwise distribution of blade loading for propeller G1 is higher in the intermediate and tip regions in comparison with the reference propeller for the advance ratio $J=1$ corresponding to maximum efficiency.

Propeller G2 has a linear pitch angle distribution along the blade, and one can observe that it shows lower coefficients of thrust and power with nearly the same efficiency in comparison with propeller G1, but it shows higher blade loading at the intermediate region and lower blade loading at the tip region in comparison with propeller G1.

To investigate the effect of airfoil section, two rotors were calculated based on the airfoils Göttingen 796 and generalized Joukowski, respectively. It was found that the thrust and

the power coefficients and the efficiency of the generalized Joukowski-based propeller are greater than the respective coefficients of Göttingen-based propeller for advanced ratio $J=0.65$ and higher.

The efficiency curves do not show any noticeable variation due to using multiple airfoils along the blade. Also from the predicted results, the propeller with three airfoils along the blades shows bigger loading at the root region and lower loading at the tip than that of the propeller with only single airfoil along the blade.

It was shown that correcting only tip and compressibility effects produced thrust and power coefficients which are closer to the experiments and to the predictions from the panel method. The inclusion of the hub interference effect based on the available formulation in the literature seems to penalize severely the rotor and reduce its output. The results from the present code show that the inclusion of the Prandtl corrections provides an unloading of the blade tip. A recent review realized shows that this problem is not completely sorted out and needs more analysis and more experimental measurements to quantify better the hub effects. For the present analysis, we will consider only the tip and compressibility effects.

The numerical predictions showed that the reduction in the blade loading at the tip region and its increase in the middle part of the blade can be obtained by adopting linear distribution of the pitch angle or by using tapered blade. These effects are intensified by the increase in the blade taper ratio. It is also possible to observe from the predicted results that the use of the elliptical chord distribution instead of tapered blade accentuates these effects. However, the changes in the geometry of the blade reduce the blade loading near the tip but also reduce the coefficient of thrust, torque and power at nearly constant efficiency, in comparison with the blade having the reference chord distribution.

Acknowledgements The first author wishes to thank the Conselho Nacional de Desenvolvimento Científico e Tecnológico (CNPq) for the PQ Research Grant.

References

1. Theodorsen T (1948) Theory of propellers. McGraw-Hill, New York, pp 6–15
2. Dumitrescu H, Cardos V (1998) Wind turbine aerodynamic performance by lifting line method. Int J Rot Mach 4(3):141–149. <https://doi.org/10.1155/S1023621X98000128>
3. Palmeter SM, Katz J (2010) Evaluation of a potential flow model for propeller and wind turbine design. J Aircr 47(5):1739–1746
4. Slavík S (2004) Preliminary determination of propeller aerodynamic characteristics for small aeroplanes. Acta Polytech 44(2):103–108
5. Gur O, Rosen A (2008) Comparison between blade-element models of propellers. Aeronaut J 112(1138):689–704
6. Uhlig DV, Selig MS (2008) Post stall propeller behavior at low Reynolds numbers. In: 46th AIAA Aerospace Sciences Meeting and Exhibit. 2008-0407
7. Bohorquez F, Pines D, Samuel PD (2010) Small rotor design optimization using blade element momentum theory and hover tests. J Aircr 47(1):268–283. <https://doi.org/10.2514/1.45301>
8. Khan W, Nahon M (2015) Development and validation of a propeller slipstream model for unmanned aerial vehicles. J Aircr. <https://doi.org/10.2514/1.C033118> (AIAA Early Edition)
9. Drela M (2013) XFOIL Subsonic airfoil development system, XFOIL 6.99. Massachusetts Institute of Technology, Cambridge, MA, USA. <http://web.mit.edu/drela/Public/web/xfoil/>. Accessed 12 April 2016
10. Morgado J (2016) Development of an open source software tool for propeller design in the MAATProject. University of Beira Interior, PhD Thesis, March
11. Silvestre MAR, Morgado J, Páscoa JC (2013) JBLADE: a propeller design and analysis code. In: 2013 International powered lift conference. American Institute of Aeronautics and Astronautics, Los Angeles, CA, USA. <https://doi.org/10.2514/6.2013-4220>
12. Morgado J, Abdollahzadeh M, Silvestre MAR, Páscoa JC (2015) High altitude propeller design and analysis. Aerosp Sci Technol 45:398–407. <https://doi.org/10.1016/j.ast.2015.06.011>
13. MacNeill R, Verstraete D (2017) Blade element momentum theory extended to model low Reynolds number propeller performance. Aeronaut J 121(1240):835–857. <https://doi.org/10.1017/aer.2017.32>
14. Wald QR (2006) The aerodynamics of propeller. Prog Aerosp Sci 42(2):85–128
15. Glauert H (1926) The elements of aerofoil and airscrew theory. Cambridge University Press, Cambridge, pp 199–221
16. Houghton EL, Carpenter PW, Collicott SH, Valentine DT (2013) Aerodynamics for engineering students, 6th edn. Elsevier, Amsterdam, pp 643–687
17. Wald QR (1964) The distribution of circulation on propellers with finite hubs. ASME Paper 64WA/UNT-4, Winter Annual Meeting, New York
18. Glauert H (1935) Airplane propellers, Vol IV, Div L, Chap VII. In: Durand WF (ed) Aerodynamic theory. Julius Springer, Berlin [Reprinted 1963 by Dover Publications, Inc., New York], pp 251–269
19. Hartman EP, Biermann D (1938) The aerodynamic characteristics full-scale propellers having 2, 3 and 4 blades of Clark Y and RAF 6 airfoil sections. NACA Report No. 640. Langley Memorial Aeronautical Laboratory, National Advisory Committee for Aeronautics, Langley Field, VA, USA
20. Lyon CA, Broeren AP, Giguère P, Gopalarathnam A, Selig MS (1998) Summary of low-speed airfoil data, vol 3. Department of Aeronautical and Astronautical Engineering, University of Illinois at Urbana-Champaign, SoarTech Publications, Virginia Beach, VA, USA
21. Glauert H (1924) A generalised type of Joukowski aerofoil. ARC RM No. 911

Publisher's Note Springer Nature remains neutral with regard to jurisdictional claims in published maps and institutional affiliations.